

# Complex HRRP Target Recognition Based on Phase and Amplitude Fusion Analysis

Jian-Sheng Fu\*, Hui Zu, Zhi Qiao, and Shao-Fei Wang

**Abstract**—Due to the traditional recognition researches prevalently focusing on HRRP's amplitudes while almost completely neglecting the phases, this paper attempts to directly prove the discriminant availability of HRRP's phases via two proposed fusion recognition strategies. The first strategy includes three sub-processes, respectively, based on phase cosine, phase sine and their fusion. The second strategy also includes three sub-processes, respectively, based on phases, amplitudes and their fusion. Additionally, a trigonometric function couple (TFC) method is used to reduce the phase sensitivity. Several measured experimental results indicate as follows. Firstly, employing TFC can perform much better. Secondly, the two fusion recognition sub-processes apparently outperform the corresponding sub-processes constructing them. Finally, phase information usually has a better noise immunity than amplitude information, and fusing phase information into amplitudes may improve the traditional recognition performance. Therefore, the availabilities of HRRP's phases and the two fusion strategies have been experimentally proven.

## 1. INTRODUCTION

An original high resolution range profile (HRRP), a *complex* vector, is composed of amplitude and *phase* information of coherent summations of the complex returns from target scatterers in each range cell, which represents the projection of the complex returned echoes from the target scattering centers onto the radar line-of-sight (LOS) [1, 2]. Among several kinds of the windband radar target signatures, such as 2-D and 3-D radar target images [3], HRRP is a promising signature and more easy to be acquired in actual application, but it is highly sensitive to target-aspect, time-shift and amplitude-scale variations [4–6], so how to extract robust and effective feature from the raw signal becomes a key problem in HRRP-based radar automatic target recognition (RATR). During the past decade, many measured and simulated experimental results also confirmed that some physical structure information naturally contained in complex HRRPs, such as target size [7], scatterer distribution [8, 9], amplitude fluctuation [10–16], is very beneficial to HRRP-based RATR, and accordingly, a number of statistical methods have been proposed for feature extraction and dimension reduction.

These statistical discriminant methods were generally employed to deal with HRRP's amplitudes, that is to say, their prevalent applications were designed to extract the discrimination information only from real HRRPs rather than the complex ones [2, 10–16], thereby probably losing some valuable discriminant information contained in the phases and potentially resulting in a dissatisfied recognition performance sometimes [17]. Nevertheless, in addition to these traditional applications, there has been little recognition work done via directly using the phase information of complex HRRPs due to two main reasons. One reason is the sensitivity problem. Theoretically speaking, HRRP's phases are so sensitive to target-aspect, time-shift and amplitude-scale variations that the pure phase units can be considered

---

Received 22 April 2014, Accepted 10 June 2014, Scheduled 19 June 2014

\* Corresponding author: Jian-Sheng Fu (fjs2012@126.com).

The authors are with the China Merchants Chongqing Communications Research and Design Institute Co. Ltd., Chongqing 400067, China.

containing little useful discriminant information, and therefore can be ignored in some sense [5], but no experiment at present supports this opinion. Another reason is the computation problem. Mathematically speaking, the discriminating process based on complex HRRPs usually consumes more computation and storage resources than the real's, so we ordinarily prefer real HRRPs because the huge storage requirement and computation burden always appear in HRRP-based RATR [5, 18]. Despite the two problems aforementioned summarily, Du et al. have indirectly proved the discriminant availability of HRRP's phases via comparing the recognition performance between the complex and real HRRPs [6]. However, the discriminant availability of HRRP's phases still has not been directly tested by experiment at present.

Motivated by the analysis above, the main intention of this paper is to directly prove the discriminant availability of phase information contained in complex HRRPs. Due to the higher phase sensitivity than the amplitude's in target-aspect [5], a trigonometric function couple (TFC), i.e., the cosine and sine functions, is employed to reduce its sensitivity and improve the recognition stability. Consider that the fusion recognition techniques always appear in RATR [14, 15], two fusion recognition strategies are also proposed in this paper, of which the first strategy is specially designed for phase recognition while the second is based on HRRP's phases and amplitudes. Additionally, in order to clearly analyze the two proposed strategies, linear discriminant analysis (LDA) and 1-nearest neighbor (1-NN) ruler are both employed in them to demonstrate the detailed processes [19, 20]. One view worth pointing out is that this paper is mainly used to prove the discriminant availability of HRRP's phases via testing the recognition availabilities of the proposed strategies, so application of LDA and 1-NN has little essential effect on the two strategies, that is to further say, many other similar methods can also be applied to the two strategies to test the discriminant availability of HRRP's phases.

The rest is organized as follows. In Section 2, we proceed to delve into the details of the first fusion recognition strategy. In Section 3, the second fusion recognition strategy is detailed based on HRRP's phases and amplitudes. In Section 4, we apply the two strategies in the measured experiments to evaluate the recognition performances. Finally, some conclusions are made in Section 5.

## 2. THE FIRST FUSION RECOGNITION STRATEGY BASED ON HRRP'S PHASES

Throughout this paper, consider a set of  $M$  complex HRRPs  $\{\mathbf{X}|x_i, i = 1, 2, \dots, M\}$  defined on a  $2n$ -dimensional complex space  $\mathbb{F}^{2n}$ , containing  $g$  classes with each class consisting of  $m_\xi$  ( $\xi = 1, 2, \dots, g$ ) training samples. Let  $\{\mathbf{X}_\xi|\mathbf{x}_{\xi,j}, j = 1, 2, \dots, m_\xi\}$ ,  $\{\mathbf{A}_\xi|\mathbf{a}_{\xi,j}, j = 1, 2, \dots, m_\xi\}$  and  $\{\Theta_\xi|\theta_{\xi,j}, j = 1, 2, \dots, m_\xi\}$ , respectively, denote the complex, amplitude and phase subsets of Class  $\xi$ , here the column vectors  $\mathbf{x}_{\xi,j}$ ,  $\mathbf{a}_{\xi,j}$  and  $\theta_{\xi,j}$  are given by

$$\begin{cases} \mathbf{x}_{\xi,j} = [x_{\xi,j,1}, x_{\xi,j,2}, \dots, x_{\xi,j,2n}]^T \\ \quad = [a_{\xi,j,1}e^{i*\theta_{\xi,j,1}}, a_{\xi,j,2}e^{i*\theta_{\xi,j,2}}, \dots, a_{\xi,j,2n}e^{i*\theta_{\xi,j,2n}}]^T \\ \mathbf{a}_{\xi,j} = [a_{\xi,j,1}, a_{\xi,j,2}, \dots, a_{\xi,j,2n}]^T \\ \theta_{\xi,j} = [\theta_{\xi,j,1}, \theta_{\xi,j,2}, \dots, \theta_{\xi,j,2n}]^T \end{cases} \quad \begin{matrix} (j = 1, 2, \dots, m_\xi) \\ (\xi = 1, 2, \dots, g) \end{matrix}, \quad (1)$$

where the mathematical notation  $i$  is defined as the imaginary symbol throughout this paper, thus we have  $M = \sum_{\xi=1}^g m_\xi$ ,  $\mathbf{X} = [\mathbf{X}_1, \mathbf{X}_2, \dots, \mathbf{X}_g]$ ,  $\mathbf{A} = [\mathbf{A}_1, \mathbf{A}_2, \dots, \mathbf{A}_g]$  and  $\Theta = [\Theta_1, \Theta_2, \dots, \Theta_g]$ .

Let's analyze the formation mechanism of HRRP [1, 5, 6]. Supposing that there exists a radar target denoted by  $\varphi$ , its HRRP can be considered as a discrete sampling sequence of the target electromagnetic echo  $\phi(f)$ , which can be approximated as a scatterer model of the radar center frequency  $f$ , that is,

$$\phi(f) = \sum_{\xi=1}^Q \alpha_\xi \exp(i * 2\pi f \tau_\xi), \quad (2)$$

where  $Q$  denotes  $\varphi$ 's scatterer number, and accordingly,  $\alpha_\xi$  and  $\tau_\xi$ , respectively, denote the scattering intensity and arrival time of the  $\xi^{\text{th}}$  scatterer. Then the HRRP  $\mathbf{x}$  can be constructed by  $\mathbf{x} =$

$[x_1, x_2, \dots, x_P]^T$ , here  $x_\kappa$  is given by

$$x_\kappa = \phi_\kappa(f) = \sum_{\eta=1}^{Q_\kappa} \alpha_{\kappa,\eta} \exp(i * 2\pi f \tau_{\kappa,\eta}) = \alpha_\kappa \exp(i * \theta_\kappa) \quad (\kappa = 1, 2, \dots, P), \quad (3)$$

where  $P$  denotes  $\varphi$ 's range resolution cell (RRC) number, and  $Q_\kappa$ ,  $\alpha_\kappa$  and  $\theta_\kappa$ , respectively, denote the scatterer number, scattering intensity and angle in the  $\kappa^{\text{th}}$  RRC. Accordingly,  $\alpha_{\kappa,\xi}$  and  $\tau_{\kappa,\xi}$ , respectively, denote the scattering intensity and arrival time of the  $\eta^{\text{th}}$  scatterer in the  $\kappa^{\text{th}}$  RRC.

Generally speaking, the amplitude and phase of target scatterer can both reflect the target physical architecture in electromagnetic form, so HRRP's amplitude and phase both contain some valuable information for recognition. In term of physical significance within a certain RRC as demonstrated by (3), HRRP's amplitude can be considered as the energy accumulation in space axis while phase is the momentum accumulation in time axis. That is to say, their physical significances are very different, so the discriminant information contained in them is also different. Only using amplitude information for recognition is equivalently based on the mathematical assumption that all phases are strictly set to a single value, while actually the phases may contain some target architecture information which does not exist in the amplitudes. Due to the higher aspect-sensitivity of phase than the amplitude's [1, 5, 6], the recognition performance of phase is acceptably inferior to the amplitude's, but fusing phase information into amplitudes may improve the recognition performance more or less. Furthermore, in terms of electromagnetic wave, its energy can be easily interfered by mutable electromagnetic environment while its frequency always performs relatively stable in many mediums, and as a result, phase information may have a better noise immunity than amplitude information.

## 2.1. The Pretreatment of HRRP's Phases

Different from Du's revealing the discriminant availability of HRRP's phases indirectly [6], this paper attempts to directly dispose the pure phase information. Enlightened by HRRP's expression formula,

$$x_{\xi,j,i} = a_{\xi,j,i} (\cos(\theta_{\xi,j,i}) + i * \sin(\theta_{\xi,j,i})) \quad (i = 1, 2, \dots, 2n; \quad j = 1, 2, \dots, m_\xi; \quad \xi = 1, 2, \dots, g), \quad (4)$$

we define a TFC method in this paper to directly deal with the phases by

$$\begin{cases} \mathbf{C}_\xi = (\cos(\theta_{\xi,j,i}))_{(i=1,2,\dots,2n; j=1,2,\dots,m_\xi)} = \cos(\bar{\Theta}_\xi) \\ \mathbf{S}_\xi = (\sin(\theta_{\xi,j,i}))_{(i=1,2,\dots,2n; j=1,2,\dots,m_\xi)} = \sin(\bar{\Theta}_\xi) \end{cases} \quad (\xi = 1, 2, \dots, g), \quad (5)$$

where the matrices  $\mathbf{C}_\xi$  and  $\mathbf{S}_\xi$ , respectively, denote the cosine and sine results of the matrix  $\bar{\Theta}_\xi$ . Accordingly, the cosine training space  $\mathbf{C}$  and the sine training space  $\mathbf{S}$  are constructed by

$$\mathbf{C} = [\mathbf{C}_1, \mathbf{C}_2, \dots, \mathbf{C}_g] \quad \text{and} \quad \mathbf{S} = [\mathbf{S}_1, \mathbf{S}_2, \dots, \mathbf{S}_g]. \quad (6)$$

Let's consider TFC's effect on phase-preprocessing. According to the theoretical analysis provided above and in [1–6], HRRP's phases are useful for recognition. But in actual extraction by inverse trigonometric transform, the radian values of all elements in  $\bar{\Theta}$  are mathematically limited to the fluctuation range  $[-\pi, \pi]$ . Through TFC, the fluctuation range of HRRP's phases is comparatively changed from the actual  $[-\pi, \pi]$  to the virtual  $[-\pi/2, \pi/2]$ . As a result, it equivalently truncates the fluctuation amplitude of  $\bar{\Theta}$  by two times, so it can reduce the phase sensitivity in some sense. Furthermore, as a nonlinear mapping, TFC may decompose more information beneficial to recognition. Although TFC may reduce the phase sensitivity and improve the recognition stability via enriching the fluctuation characteristics of HRRP's phases, one view worth pointing out is that it is at the expense of some discriminant information contained in HRRP's phases [17]. Note that the main intention of this paper is to directly prove the discriminant availability of HRRP's phases, and TFC is rationally accepted even though there really exists some useful discriminant information probably losing.

Due to the high time-shift and amplitude-scale sensitivity of HRRP [1–6], some methods should be adopted to pretreat the trigonometric matrixes  $\mathbf{C}_\xi$  and  $\mathbf{S}_\xi$ . In this paper, a simple method mentioned in [2] is specially suggested for the following pretreatment. Let's suppose that, with the help of this method, we have obtained the preprocessed matrixes  $\bar{\mathbf{C}}_\xi$  and  $\bar{\mathbf{S}}_\xi$  from  $\mathbf{C}_\xi$  and  $\mathbf{S}_\xi$ , respectively, then the cosine training space  $\bar{\mathbf{C}}$  and sine training space  $\bar{\mathbf{S}}$  are arranged by

$$\bar{\mathbf{C}} = [\bar{\mathbf{C}}_1, \bar{\mathbf{C}}_2, \dots, \bar{\mathbf{C}}_g] \quad \text{and} \quad \bar{\mathbf{S}} = [\bar{\mathbf{S}}_1, \bar{\mathbf{S}}_2, \dots, \bar{\mathbf{S}}_g]. \quad (7)$$

## 2.2. The Recognition of HRRP's Phases

Once acquiring the preprocessed matrixes  $\bar{\mathbf{C}}$  and  $\bar{\mathbf{S}}$  from HRRP's phases, we proceed to delve into the recognition details. Through the LDA algorithm, we obtain the feature projection subspaces (FPSs)  $\mathbf{U}^C$  and  $\mathbf{U}^S$  from the training spaces  $\bar{\mathbf{C}}$  and  $\bar{\mathbf{S}}$ , respectively. Then the feature subspaces  $\bar{\mathbf{C}}_\xi$  and  $\bar{\mathbf{S}}_\xi$  of Class  $\xi$  can be calculated by

$$\bar{\mathbf{C}}_\xi = \left( (\bar{\mathbf{C}}_\xi)^T \mathbf{U}^C \right)^T \quad \text{and} \quad \bar{\mathbf{S}}_\xi = \left( (\bar{\mathbf{S}}_\xi)^T \mathbf{U}^S \right)^T \quad (\xi = 1, 2, \dots, g), \quad (8)$$

where the matrixes  $\bar{\mathbf{C}}_\xi$  and  $\bar{\mathbf{S}}_\xi$ , respectively, denote the cosine and sine feature subspaces of Class  $\xi$ . Similarly, the cosine feature space  $\bar{\mathbf{C}}$  and sine training space  $\bar{\mathbf{S}}$  can be constructed by

$$\bar{\mathbf{C}} = \left[ \bar{\mathbf{C}}_1, \bar{\mathbf{C}}_2, \dots, \bar{\mathbf{C}}_g \right] \quad \text{and} \quad \bar{\mathbf{S}} = \left[ \bar{\mathbf{S}}_1, \bar{\mathbf{S}}_2, \dots, \bar{\mathbf{S}}_g \right]. \quad (9)$$

Generally speaking, the main application of the feature subspaces  $\bar{\mathbf{C}}_\xi$  and  $\bar{\mathbf{S}}_\xi$  is for template-matching, which is usually divided into three solving steps as follows. Firstly, given a test HRRP  $\mathbf{x}^\Omega$  and its phase vector  $\theta^\Omega$ , we can obtain its feature vectors  $\bar{\mathbf{c}}^\Omega$  and  $\bar{\mathbf{s}}^\Omega$  along with the solution process above, where  $\bar{\mathbf{c}}^\Omega$  and  $\bar{\mathbf{s}}^\Omega$ , respectively, denote the cosine and sine features of the phase vector  $\theta^\Omega$ . Secondly, under the 1-NN ruler, we can obtain its nearest Euclidean distances (NEDs)  $d_\xi^{\Omega C}$  and  $d_\xi^{\Omega S}$ , where the values  $d_\xi^{\Omega C}$  and  $d_\xi^{\Omega S}$ , respectively, denote the NED between  $\bar{\mathbf{c}}^\Omega$  and  $\bar{\mathbf{C}}_\xi$ , and the NED between  $\bar{\mathbf{s}}^\Omega$  and  $\bar{\mathbf{S}}_\xi$ . Finally, the test sample  $\mathbf{x}^\Omega$  can be classified by

$$\Phi^{\Omega C} = \arg \min_{\xi=1,2,\dots,g} d_\xi^{\Omega C} \quad \text{and} \quad \Phi^{\Omega S} = \arg \min_{\xi=1,2,\dots,g} d_\xi^{\Omega S}, \quad (10)$$

where the attribution  $\Phi^{\Omega C}$  denotes that  $\mathbf{x}^\Omega$  belongs to Class  $\Phi^{\Omega C}$  under the phase cosine pattern, and the attribution  $\Phi^{\Omega S}$  denotes that  $\mathbf{x}^\Omega$  belongs to Class  $\Phi^{\Omega S}$  under the phase sine pattern.

Enlightened by the NED's fusion technique in [10], we proceed to analyze the fusion recognition problem in the first strategy. Supposing that the amplitudes of HRRPs have been all strictly set to 1, and then compared with HRRP's expression formula as given by (4), we can find that the phase cosine space  $\bar{\mathbf{C}}$  can be considered as a real mapping space of TFC while  $\bar{\mathbf{S}}$  is imaginary. Accordingly, the value  $d_\xi^{\Omega C}$  is the NED measurement in the real space  $\bar{\mathbf{C}}_\xi$  while  $d_\xi^{\Omega S}$  is calculated in the imaginary space  $\bar{\mathbf{S}}_\xi$ . According to plural calculation theory, the two different NEDs can be fused by

$$d_\xi^{\Omega \Theta} = \|d_\xi^{\Omega C} + i * d_\xi^{\Omega S}\| = \sqrt{\left(d_\xi^{\Omega C}\right)^2 + \left(d_\xi^{\Omega S}\right)^2} \quad (\xi = 1, 2, \dots, g), \quad (11)$$

where the value  $d_\xi^{\Omega \Theta}$  denotes the fusion NED between the test sample  $\mathbf{x}^\Omega$  and Class  $\xi$  under the first strategy. Then we can obtain its corresponding attribution  $\Phi^{\Omega \Theta}$  under the 1-NN ruler.

## 3. THE SECOND FUSION RECOGNITION STRATEGY BASED ON HRRP'S PHASES AND AMPLITUDES

Based on HRRP's different sub-information units, i.e., phases and amplitudes, the proposed strategy is divided into two sub-sections as follows.

### 3.1. The Recognition of HRRP's Amplitudes

Obviously, HRRP's amplitude subset is equivalent to real HRRPs [2]. Due to the massive recognition researches focusing on real HRRPs during past years [10–16], the discriminant process of HRRP's amplitudes is moderately reduced as that. Firstly, through the preprocessed method offered in [2], we obtain the training space  $\bar{\mathbf{A}}$  from the original space  $\mathbf{A}$ . Secondly, with the help of LDA, we obtain the FPS  $\mathbf{U}^A$  from the training space  $\bar{\mathbf{A}}$ . Finally, we obtain the feature subspace  $\bar{\mathbf{A}}_\xi$  of Class  $\xi$  by

$$\bar{\mathbf{A}}_\xi = \left( (\bar{\mathbf{A}}_\xi)^T \mathbf{U}^A \right)^T \quad (\xi = 1, 2, \dots, g), \quad (12)$$

and then arrange the feature space  $\bar{\bar{\mathbf{A}}} = [\bar{\bar{\mathbf{A}}}_1, \bar{\bar{\mathbf{A}}}_2, \dots, \bar{\bar{\mathbf{A}}}_g]$ , where the matrix  $\bar{\bar{\mathbf{A}}}_\xi$  denotes the training space of Class  $\xi$ . For the test sample  $\mathbf{x}^\Omega$  and its original amplitude vector  $\mathbf{a}^\Omega$ , we can similarly obtain its amplitude feature vector  $\bar{\bar{\mathbf{a}}}^\Omega$  and attribution  $\Phi^{\Omega\Lambda}$  under the 1-NN ruler.

### 3.2. The Recognition of HRRP's Phases and Amplitudes

Motivated by the double-layered feature extraction method provided in [14], we proceed to the second-layered discriminant analysis. With respect to the feature spaces  $\bar{\bar{\mathbf{C}}}_\xi$ ,  $\bar{\bar{\mathbf{S}}}_\xi$  and  $\bar{\bar{\mathbf{A}}}_\xi$  obtained in front, even though they can be structured as a training space for discriminant, their distributions are different in terms of statistical scale, so some pretreatment must be adopted to normalize them. As the traditional statistical measurement, standard deviation is suggested in this paper to normalize the feature spaces. Let's suppose that the values  $\sigma_\xi^C$ ,  $\sigma_\xi^S$  and  $\sigma_\xi^A$ , respectively, denote the standard deviations of the feature spaces  $\bar{\bar{\mathbf{C}}}_\xi$ ,  $\bar{\bar{\mathbf{S}}}_\xi$  and  $\bar{\bar{\mathbf{A}}}_\xi$ , then the overall standard deviations can be given by

$$\sigma^C = \sqrt{\sum_{\xi=1}^g (\sigma_\xi^C)^2 / g}, \quad \sigma^S = \sqrt{\sum_{\xi=1}^g (\sigma_\xi^S)^2 / g} \quad \text{and} \quad \sigma^A = \sqrt{\sum_{\xi=1}^g (\sigma_\xi^A)^2 / g}, \quad (13)$$

where the values  $\sigma^C$ ,  $\sigma^S$  and  $\sigma^A$ , respectively, denote the overall standard deviations of the feature spaces  $\bar{\bar{\mathbf{C}}}$ ,  $\bar{\bar{\mathbf{S}}}$  and  $\bar{\bar{\mathbf{A}}}$ . Accordingly, the normalized feature spaces are constructed by

$$\begin{cases} \bar{\bar{\mathbf{X}}}_\xi = \left[ \left( \bar{\bar{\mathbf{C}}}_\xi / \sigma^C \right)^T, \left( \bar{\bar{\mathbf{S}}}_\xi / \sigma^S \right)^T, \left( \bar{\bar{\mathbf{A}}}_\xi / \sigma^A \right)^T \right]^T \\ \bar{\bar{\mathbf{X}}} = [\bar{\bar{\mathbf{X}}}_1, \bar{\bar{\mathbf{X}}}_2, \dots, \bar{\bar{\mathbf{X}}}_g] \end{cases} \quad (\xi = 1, 2, \dots, g), \quad (14)$$

where matrix  $\bar{\bar{\mathbf{X}}}_\xi$  denotes the second-layered training subspace of Class  $\xi$ , and matrix  $\bar{\bar{\mathbf{X}}}$  denotes the total second-layered training space.

Once obtaining the training space  $\bar{\bar{\mathbf{X}}}$ , we apply it to calculate the FPS  $\bar{\bar{\mathbf{U}}}$  through directly employing the LDA algorithm. Then the feature subspace  $\mathbf{Y}_\xi$  of Class  $\xi$  is given by

$$\mathbf{Y}_\xi = \left( \left( \bar{\bar{\mathbf{X}}}_\xi \right)^T \bar{\bar{\mathbf{U}}} \right)^T \quad (\xi = 1, 2, \dots, g). \quad (15)$$

Let's analyze the logical relations among the FPSs  $\mathbf{U}^C$ ,  $\mathbf{U}^S$ ,  $\mathbf{U}^A$  and  $\bar{\bar{\mathbf{U}}}$ . Evidently, the FPSs  $\mathbf{U}^C$ ,  $\mathbf{U}^S$  and  $\mathbf{U}^A$  are used to extract the feature subspaces  $\bar{\bar{\mathbf{C}}}$ ,  $\bar{\bar{\mathbf{S}}}$  and  $\bar{\bar{\mathbf{A}}}$  from the training spaces  $\bar{\mathbf{C}}$ ,  $\bar{\mathbf{S}}$  and  $\bar{\mathbf{A}}$ , respectively, while the normalizations of the feature subspaces  $\bar{\bar{\mathbf{C}}}$ ,  $\bar{\bar{\mathbf{S}}}$  and  $\bar{\bar{\mathbf{A}}}$  are synthetically used to obtain the FPS  $\bar{\bar{\mathbf{U}}}$  by the LDA algorithm. Similar to the analysis in [14], we can construct a projection matrix to synthesize these four FPSs as a global FPS. Supposing that the dimensions of the FPSs  $\mathbf{U}^C$ ,  $\mathbf{U}^S$  and  $\mathbf{U}^A$ , respectively, are  $n \times N^C$ ,  $n \times N^S$  and  $n \times N^A$ , then the global FPS  $\mathbf{U}$  is given by

$$\mathbf{U} = \begin{bmatrix} \mathbf{U}^C / \sigma^C & \mathbf{0}_{n, N^S} & \mathbf{0}_{n, N^A} \\ \mathbf{0}_{n, N^C} & \mathbf{U}^S / \sigma^S & \mathbf{0}_{n, N^A} \\ \mathbf{0}_{n, N^C} & \mathbf{0}_{n, N^S} & \mathbf{U}^A / \sigma^A \end{bmatrix} \bar{\bar{\mathbf{U}}}, \quad (16)$$

where the zero sub-space  $\mathbf{0}_{i,j}$  is defined as a  $i \times j$  matrix with all elements strictly setting to 0. Accordingly, the training subspace  $\bar{\bar{\mathbf{X}}}_\xi$  of Class  $\xi$  is constructed by  $\bar{\bar{\mathbf{X}}}_\xi = [(\bar{\bar{\mathbf{C}}}_\xi)^T, (\bar{\bar{\mathbf{S}}}_\xi)^T, (\bar{\bar{\mathbf{A}}}_\xi)^T]^T$ , and then the feature subspace  $\mathbf{Y}_\xi$  can be equivalently obtained by

$$\mathbf{Y}_\xi = \left( \left( \bar{\bar{\mathbf{X}}}_\xi \right)^T \mathbf{U} \right)^T \quad (\xi = 1, 2, \dots, g). \quad (17)$$

Obviously, the training subspace  $\bar{\bar{\mathbf{X}}}_\xi$  contains not only the phase information  $\bar{\bar{\mathbf{C}}}_\xi$  and  $\bar{\bar{\mathbf{S}}}_\xi$ , but also the phase information  $\bar{\bar{\mathbf{A}}}_\xi$ . As a comprehensive mapping, the FPS  $\mathbf{U}$  fuses the phase and amplitude information simultaneously.

For the test sample  $\mathbf{x}^\Omega$ , we can similarly construct its first-layered test vector  $\bar{\bar{\mathbf{x}}}^\Omega$  along with the corresponding steps, and accordingly, its feature vector  $\mathbf{y}^\Omega$  can be obtained by  $\mathbf{y}^\Omega = ((\bar{\bar{\mathbf{x}}}^\Omega)^T \mathbf{U})^T$ . Then under the 1-NN ruler, we can easily obtain its attribution  $\Phi^\Omega$ .

## 4. EXPERIMENTS AND ANALYSES

The original HRRP data used to evaluate the recognition performance was measured by a C-band ISAR radar with bandwidth 400 MHz [4–7, 10–14], including the 1<sup>st</sup>, 2<sup>nd</sup>, 4<sup>th</sup> and 7<sup>th</sup> segments of An-16, the 1<sup>st</sup>, 2<sup>nd</sup>, 4<sup>th</sup> and 7<sup>th</sup> segments of Jiang (Cessna Citation S/II), and the 1<sup>st</sup>, 2<sup>nd</sup>, 4<sup>th</sup> and 5<sup>th</sup> segments of Yak-42, with each segment containing 260 complex HRRPs. In order to evaluate the proposed strategies, two experimental datasets are designed as follows. One dataset is labeled by Dataset I, including the 4<sup>th</sup> segment of An-16, 7<sup>th</sup> segment of Jiang, and 1<sup>st</sup> segment of Yak-42, with each segment providing 240 HRRPs, so Dataset I contains 720 HRRPs in total. Another dataset is labeled by Dataset II, including four segments of each airplane, with each airplane providing 1000 HRRPs, so Dataset II contains 3000 HRRPs in total. Obviously, Dataset I has a better data continuity, while Dataset II contains more information of target-aspect and amplitude-scale variations.

In accordance with the front analysis in Sections 2 and 3, this paper provides five recognition sub-processes in the two proposed strategies. Via classifying the test sample  $\mathbf{x}^\Omega$  by the five sub-processes, we can obtain five different attributions, i.e.,  $\Phi^{\Omega C}$ ,  $\Phi^{\Omega S}$ ,  $\Phi^{\Omega \Theta}$ ,  $\Phi^{\Omega A}$  and  $\Phi^\Omega$ , and accordingly, the recognition sub-processes are labeled by “phase cosine”, “phase sine”, “phase fusion”, “amplitude” and “global fusion” respectively in the experiments. Additionally, similar to the “amplitude” recognition sub-process, the HRRP’s phase vectors are also used for a performance comparison, and the corresponding recognition sub-process is labeled by “phase” in the experiments.

### 4.1. The Experiment on Feature Spaces

According to the description in Section 2.2, there exist some feature spaces used for template-matching. Actually, the feature spaces can directly affect the recognition results. In order to evaluate the feature performances of the “global fusion”, “amplitude”, “phase cosine” and “phase sine” sub-process, Dataset I is recommended in the experiment, and accordingly, the training feature spaces are depicted in Figure 1. For a comparison support, the correct recognition rates (CRRs) based on Dataset I are also listed in Table 1. Based on the experimental results, some analyses are given as follows.

Firstly, the feature discriminant degrees in Figure 1 are labeled from high to low by “global fusion”, “amplitude”, “phase sine” and “phase cosine”, among which the “phase sine” and “phase cosine” sub-processes have a similar discriminant degree and actually difficult to be distinguished. Compared with the relative CRRs offered in Table 1, we can find that a better training discriminant degree always obtains a higher CRR.

Secondly, in terms of the sample concentration ratios, “amplitude” apparently outperforms “phase cosine” and “phase sine”, and as their fusion, “global fusion” performs the best. Furthermore, a better sample concentration ratio always means a higher CRR of this target. For example, as shown in Figure 1(b), the sample concentration ratios of three airplanes are labeled from high to low by Jiang, Yak-24 and An-26, and accordingly, their CRRs are also the same sequence as shown in Table 1.

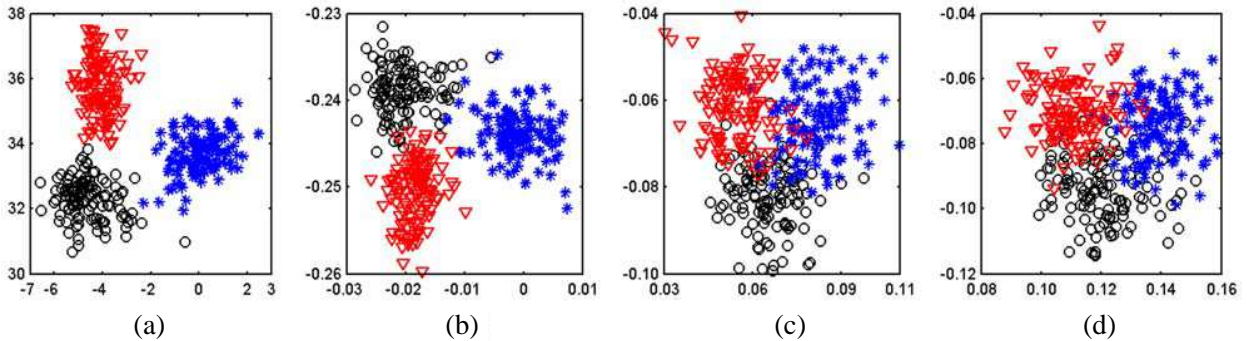


**Figure 1.** Training feature distributions in different recognition sub-processes based on Dataset I at sampling interval 2. (a) In “global fusion” recognition sub-process. (b) In “amplitude” recognition sub-process. (c) In “phase cosine” recognition sub-process. (d) In “phase sine” recognition sub-process. (“O”: An-26, “\*”: Jiang, “∇”: Yak-42.).

**Table 1.** Each target’s CRRs (%) by six recognition sub-processes.

fusion strategy	recognition sub-process	experiment on Dataset I at interval 2				experiment on Dataset II at interval 4			
		An-16	Jiang	Yak-24	average	An-16	Jiang	Yak-24	average
second	global fusion	83.33	95.00	83.33	87.22	74.93	85.20	83.20	81.11
	amplitude	86.67	95.00	74.17	85.28	73.60	81.20	78.13	77.64
first	phase fusion	54.17	70.83	54.17	59.72	51.73	60.00	68.53	60.09
	phase cosine	54.17	55.83	50.83	53.61	48.80	51.87	62.00	54.22
	phase sine	49.17	65.00	57.50	57.22	47.07	56.40	64.53	56.00
other	phase	42.50	41.67	43.33	42.50	48.80	50.27	48.00	47.69

### 4.2. The Experiment on Sampling Intervals

To evaluate the recognition performance on HRRP’s target-aspect variations, this experiment is designed operating under different sampling intervals. Dataset II is suggested in the experiment, among which the training set is selected at interval  $k$ , and the rest is used as the test set, here  $k = 2, 3, \dots, 15$ . Through altering the interval  $k$ , we can change the target-aspect differences between the training set and the test set, and accordingly, obtain the CRRs of the six recognition sub-processes, as depicted in Figure 2. Then some analyses are given as follows.

Firstly, let’s consider the adverse influence of target-aspect sensitivity in the experiment. Due to the high target-aspect sensitivity of HRRPs, all the average CRR curves in Figure 2 show a downward trend along with the sampling interval increasing. Although decreasing the sampling interval may improve the recognition performance, it may also increase the storage requirement and computation burden synchronously. Actually, it is a dilemma problem in HRRP-based RATR.

Secondly, let’s analyze the experimental performance of HRRP’s phases. As described above, there are four recognition sub-processes based on pure phase information, among which the “phase”, “phase sine” and “phase cosine” sub-processes are selected for analysis. From Figure 2 we can find that the average CRRs of “phase cosine” and “phase sine” are both evidently higher than that of “phase”, thus the availability of the TFC method has been tested. Furthermore, the average CRRs of “phase” are much higher than the blind recognition rate 33.33% at all sampling interval points, so HRRP’s phases must contain some useful discriminant information.

Thirdly, let’s analyze the experimental performance of the first strategy. From Figure 2 we can find that the average CRRs of “phase fusion” are apparently higher than those of “phase cosine” and “phase sine” at all sampling interval points, while the CRR curve of “phase cosine” is interlaced with that of

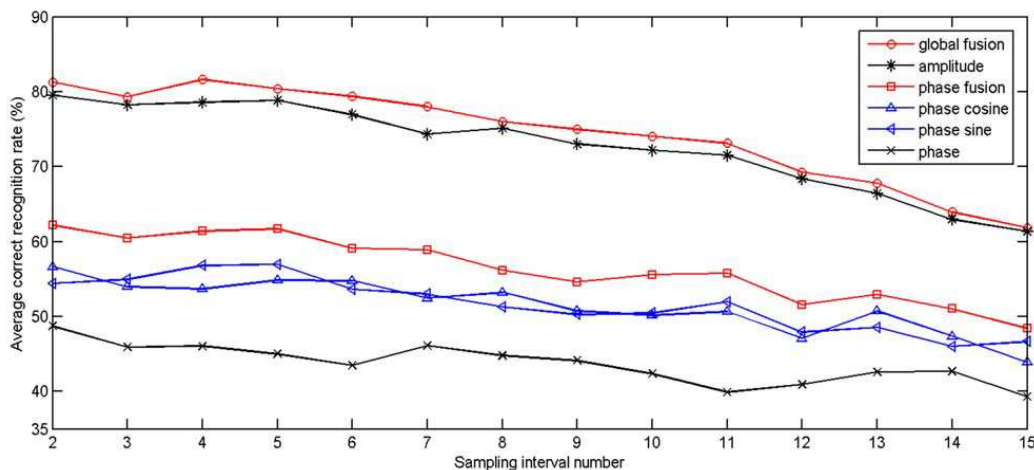


**Figure 2.** Average CRRs versus sampling interval number based on Dataset II.

“phase sine”. This phenomenon indicates that “phase cosine” and “phase sine” are complementary in some sense and can be efficiently fused. As a result, the recognition availability of the first strategy has been experimentally proven.

Finally, let’s analyze the experimental performance of the second strategy. From Figure 2 we can find that although the average CRRs of “phase fusion” are significantly lower than the corresponding CRRs of “amplitude” due to the higher phase sensitivity than the amplitude’s in target-aspect, “global fusion” generally outperforms “phase fusion” and “amplitude”, and the CRR differences between them are apparent at most sampling interval points but slightly obscure at another several points. One opinion worth pointing out is that since fusing phase and amplitude information can improve overall recognition performance, phases must contain some useful discriminant information which does not exist in amplitudes. Therefore, the availability of the second strategy has been experimentally proven.

### 4.3. The Experiments on Noise Disturbances

In order to obtain a general recognition performance of noise disturbance, a series of simulated white noises are added to the inphase and quadrature components of Dataset I and Dataset II [2], with each signal noise ratio (SNR) repeating 100 times to obtain the average, as shown in Figure 3. Meanwhile, the CRRs of the three measured airplanes under the noiseless circumstance are listed in Table 1. Taking into account actual application, the noise disturbance analyses are mainly focused on the SNR sensitive area between 10 and 30 dB [18]. Then some analyses are given as follows.

Firstly, let’s consider the general effect of noise disturbance in the two experiments. Although the experimental databases are different, the recognition results are similar, as shown in Figures 3(a) and (b). With the SNR increasing, all the average CRRs increase accordingly. When the SNR surpasses 30 dB, compared with the relative CRRs in Table 1, we can find that the noise disturbance makes a slight impact on the recognition results, and all the average CRRs keep a relatively stable condition. When the SNR varies from 30 dB to 20 dB, the average CRR curves of “global fusion” and “amplitude” drop significantly, while the other CRR curves still keep relatively stable. When the SNR varies from 20 dB to 10 dB, all the average CRRs drop sharply. When the SNR varies from 10 to 5 dB, all the average CRRs keep a downward trend in a low recognition rate zone. Most attentively, in terms of noise immunity, the phase information performs much better than the amplitude information in the two

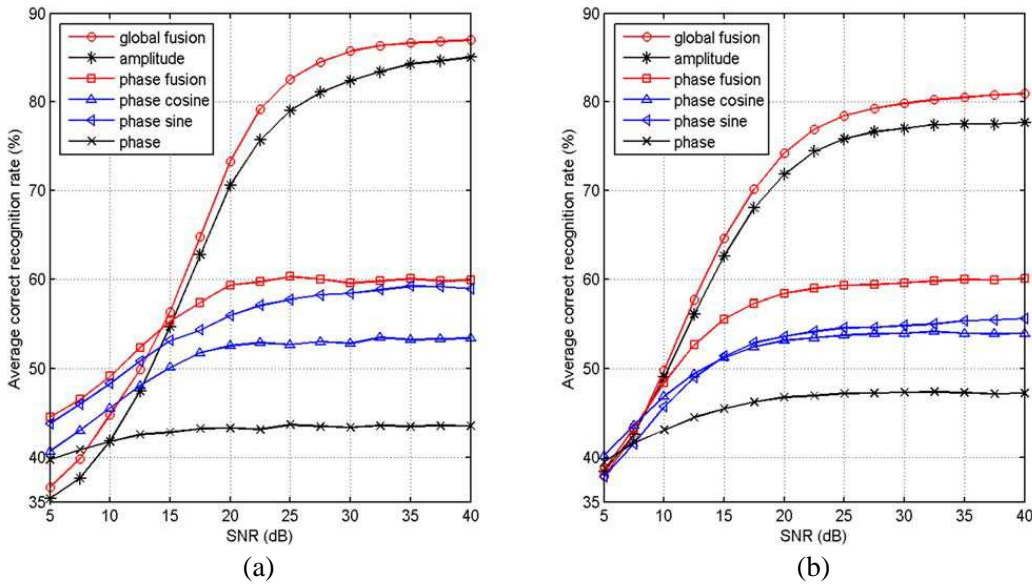


**Figure 3.** Average CRRs versus SNR. (a) Average CRRs varying with SNR in the experiment based on Dataset I at sampling interval 2. (b) Average CRRs varying with SNR in the experiment based on Dataset II at sampling interval 4.

experiments, which experimentally confirms the result of theoretical analysis in Section 2.

Secondly, let's analyze the experimental performance of HRRP's phases. From Figure 3 we can find that the average CRRs of "phase cosine" and "phase sine" are both higher than that of "phase" at almost all SNR points, thus the availability of TFC has been tested. Furthermore, with the SNR decreasing, the average CRRs of "phase cosine", "phase sine" and "phase" also decrease. When the SNR arrives at 5 dB, their CRRs are all close to the blind recognition rate 33.33%. This metabolic phenomenon evidently indicates that HRRP's phases must contain some useful discriminant information.

Thirdly, let's analyze the experimental performance of the first strategy. From Figure 3 we can find that as the fusion of "phase cosine" and "phase sine", the "phase fusion" sub-process outperforms them almost at all SNR points, especially in the SNR region between 10 and 40 dB. Thus the recognition availability of the proposed strategy has been experimentally proven.

Finally, let's analyze the experimental performance of the second strategy. In both experiments, when the SNR surpasses 15 dB, the average CRR of "global fusion" is apparently higher than those of "phase fusion" and "amplitude". With respect to the average CRRs in Figure 3(a), when the SNR is less than 15 dB, "global fusion" is superior to "amplitude" while inferior to "phase fusion". Also a similar performance can be found in Figure 3(b). Here a simple view is provided to explain this phenomenon as that in terms of noise immunity, the traditional methods applied in the second strategy can outperform the corresponding applications only using the amplitudes.

## 5. CONCLUSIONS

Generally, an original HRRP contains both amplitudes and phases, but the traditional recognition researches prevalently focus on the amplitudes while almost completely neglect the phases. To directly demonstrate the discriminant availability of HRRP's phases, two fusion recognition strategies are proposed as follows. The first strategy includes three recognition sub-processes, respectively, based on phase cosine, phase sine and their fusion. The second strategy also includes three recognition sub-processes, respectively, based on phases, amplitudes and their fusion. Additionally, a TFC phase-pretreated method is used in the first strategy to reduce the phase sensitivity. In terms of recognition performance on feature space, aspect-sensitivity and noise immunity, experimental results on the measured HRRP databases indicate as follows. Firstly, with respect to the first strategy, the recognition sub-processes applying the TFC method are apparently superior to that directly using the phases, and the sub-process fusing the phase cosine and sine information performs the best. Secondly, with respect to the second strategy, the recognition sub-process on phases performs a better noise immunity, but a lower CRR than that on amplitudes, and the sub-process fusing the phase and amplitude information performs the best. Finally, the phases contain some useful discriminant information which does not exist in amplitudes, and fusing the phase information into amplitudes can improve the traditional recognition on HRRP's amplitudes. Therefore, the availabilities of HRRP's phases and the two fusion strategies have been experimentally proven.

## ACKNOWLEDGMENT

This research work was partly supported by Application Development Major Project of CQ CSTC under Grant No. cstc2013yykfC30001.

## REFERENCES

1. Xing, M. and B. Bao, "The properties of range profile of aircraft," *Chin. J. Electron.*, Vol. 11, No. 1, 1-6, 2002.
2. Du, L., P. Wang, H. Liu, et al., "Bayesian spatiotemporal multitask learning for radar HRRP target recognition," *IEEE Trans. Signal Process.*, Vol. 59, No. 7, 3182-3196, 2011.
3. Han, S.-K., H.-T. Kim, S.-H. Park, and K.-T. Kim, "Efficient radar target recognition using a combination of range profile and time-frequency analysis," *Progress In Electromagnetics Research*, Vol. 108, 131-140, 2010.

4. Shi, L., P. Wang, H. Liu, et al., "Radar HRRP statistical recognition with local factor analysis by automatic Bayesian Ying-Yang harmony learning," *IEEE Trans. Signal Process.*, Vol. 59, No. 2, 610–617, 2011.
5. Du, L., H. Liu, Z. Bao, et al., "A two-distribution compounded statistical model for radar HRRP target recognition," *IEEE Trans. Signal Process.*, Vol. 54, No. 61, 2226–2238, 2006.
6. Du, L., H. Liu, Z. Bao, et al., "Radar automatic target recognition using complex high-resolution range profiles," *IET Radar Sonar Navig.*, Vol. 1, No. 1, 18–26, 2007.
7. Liao, K. and W. Yang, "Extraction of radar target length based on high resolution range profile," *Proc. — Int. Conf. Electr. Control Eng., ICECE*, 956–959, Jun. 26–28, 2010.
8. Astola, J. T., P. A. Molchanov, K. O. Egiiazarian, et al., "Reduction of aspect dependent speckle fluctuations in high-resolution radar range profiles," *Telecommun. Radio Eng.*, Vol. 69, No. 8, 687–698, 2010.
9. Zhang, R., X. Wei, X. Li, et al., "Analysis about the speckle of radar high resolution range profile," *Sci. China Technol. Sci.*, Vol. 54, No. 1, 226–236, 2011.
10. Fu, J.-S. and W.-L. Yang, "KFD-based multiclass synthetical discriminant analysis for radar HRRP recognition," *Journal of Electromagnetic Waves and Applications*, Vol. 26, No. 2–3, 169–178, 2012.
11. Zhou, D., X. Shen, and W. Yang, "Radar target recognition based on fuzzy optimal transformation using high-resolution range profile," *Pattern Recogn. Lett.*, Vol. 34, No. 3, 256–264, 2013.
12. Cheng, B., H. Liu, J. Chai, et al., "Large margin feature weighting method via linear programming," *IEEE Trans. Knowl. Data. Eng.*, Vol. 21, No. 10, 1475–1488, 2009.
13. Zhou, D., X. Shen, G. Wang, et al., "Orthogonal kernel projecting plane for radar HRRP recognition," *Neurocomputing*, Vol. 106, 61–67, 2013.
14. Fu, J.-S., K. liao, and W.-L. Yang, "Radar HRRP target recognition using multi-KFD-based LDA algorithm," *Progress In Electromagnetics Research C*, Vol. 34, 15–26, 2012.
15. Lee, S.-J., I.-S. Choil, B. Cho, E. J. Rothwell, and A. K. Temme, "Performance enhancement of target recognition using feature vector fusion of monostatic and bistatic radar," *Progress In Electromagnetics Research*, Vol. 144, No. 10, 291–302, 2014.
16. Zhang, L. and W.-D. Zhou, "Sparse ensembles using weighted combination methods based on linear programming," *Pattern Recogn.*, Vol. 44, No. 1, 97–106, 2011.
17. Fu, J., X. Deng, and W. Yang, "Radar HRRP recognition based on discriminant information analysis," *WSEAS Trans. Inf. Sci. Appl.*, Vol. 8, No. 4, 185–201, 2011.
18. Du, L., H. Liu, P. Wang, et al., "Noise robust radar HRRP target recognition based on multitask factor analysis with small training data size," *IEEE Trans. Signal Process.*, Vol. 60, No. 7, 3546–3559, 2012.
19. Swets, D. and J. Weng, "Using discriminant eigenfeatures for image retrieval," *IEEE Trans. Pattern Anal. Mach. Intell.*, Vol. 8, No. 2, 831–836, 1996.
20. Gou, J., L. Du, and T. Xiong, "Weighted  $k$ -nearest centroid neighbor classification," *J. Comput. Inf. Syst.*, Vol. 8, No. 2, 851–860, 2012.